Available online at www.sciencedirect.com
SCIENCE DIRECT
Precambrian Research 146 (2006) 1–15
Precambrian Research
www.elsevier.com/locate/precamres

Geochemistry of the 755 Ma Mundine Well dyke swarm, northwestern Australia: Part of a Neoproterozoic mantle superplume beneath Rodinia?

Xian-Hua Li [a,*], Zheng-Xiang Li [b], Michael T.D. Wingate [b], Sun-Lin Chung [c], Ying Liu [a], Guang-Chun Lin [a], Wu-Xian Li [a]

[a] *Key Laboratory of Isotope Geochronology and Geochemistry, Guangzhou Institute of Geochemistry, Chinese Academy of Sciences, P.O. Box 1131, Guangzhou 510640, China*
[b] *Tectonics Special Research Centre, School of Earth and Geographical Sciences, The University of Western Australia, Crawley, WA 6009, Australia*
[c] *Department of Geosciences, National Taiwan University, Taipei 106, Taiwan*

Received 22 September 2004; received in revised form 24 November 2005; accepted 1 December 2005

Abstract

Geochemical and Nd–Hf isotopic data are reported for dolerite samples from the Neoproterozoic (755 Ma) Mundine Well dyke swarm in northwestern Australia. These dolerites are tholeiitic in composition, crystallised from a common parental magma. Although the dolerite magma underwent varying degrees of crustal contamination during ascent and emplacement, the uncontaminated parental melt possessed geochemical and Nd isotopic characteristics, such as Nb/La ≈ 1.5, Nb/Th ≈ 15, Nb/U ≈ 50, εNd(T) ≈ 5, and εHf(T) ≈ 9 (estimated by extrapolation from geochemical correlations), that closely resemble plume-derived ocean island basalts. These features are also similar to those of dolerite dykes of similar age from Seychelles and South China. We propose that these late Neoproterozoic mafic suites may have been generated by melting of a vast asthenospheric mantle superplume that developed beneath, and led to breakup of, the Rodinia supercontinent.

Keywords: Neoproterozoic; Dolerite dykes; Northwestern Australia; Mantle superplume; Rodinia

1. Introduction

Neoproterozoic rifting and fragmentation of the supercontinent Rodinia is thought to have occurred between about 830 and 720 Ma (Powell et al., 1994; Preiss, 2000; Li et al., 2003b; Wang and Li, 2003). Global non-orogenic bimodal magmatism during this interval has been attributed to mantle plumes (Zhao et al., 1994; Park et al., 1995; Li et al., 1999) or to a mantle superplume responsible for Rodinia breakup (Li et al., 2001, 2003b; Frimmel et al., 2001). Identification of Precambrian continental plumes is difficult, however, owing to modification by younger geological processes. Most continental flood basalts have been lost to erosion, leaving mainly mafic dykes and sills with which to identify ancient mantle plumes (Ernst and Buchan, 1997, 2001).

Archean and Proterozoic rocks of the Pilbara and Gascoyne regions are intruded by an extensive swarm of dolerite (diabase) dykes named the Mundine Well dyke swarm (MDS) by Hickman and Lipple (1978). The dykes, dated at 755 ± 3 Ma (Wingate and Giddings, 2000), are mostly concentrated in the Gascoyne

* Corresponding author. Fax: +86 20 85290130/85514130.
E-mail address: lixh@gig.ac.cn (X.-H. Li).

0301-9268/$ – see front matter © 2005 Elsevier B.V. All rights reserved.
doi:10.1016/j.precamres.2005.12.007

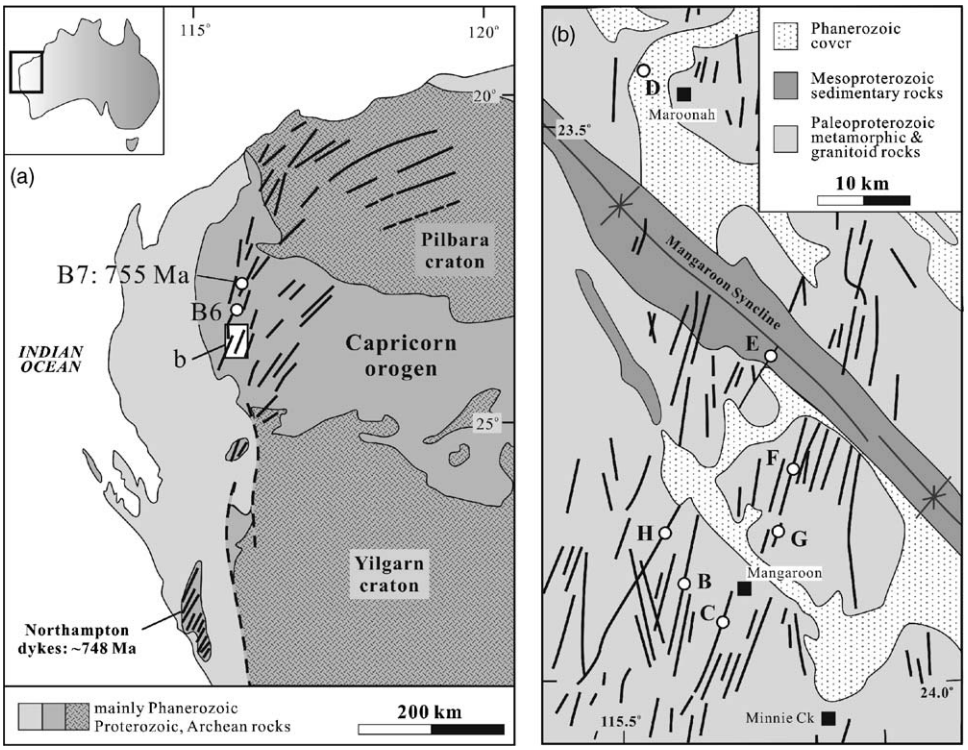

Fig. 1. Simplified geological map showing dykes of the Mundine Well swarm and sample locations (after Wingate and Giddings, 2000).

Complex and western parts of the Hamersley, Ashburton, Edmund, and Collier basins, where they trend mainly NNE (Fig. 1). They postdate regional folding of shallow-marine sedimentary and minor volcanic rocks, and 1070 Ma dolerite sills, of the Edmund and Collier Groups (Wingate and Giddings, 2000). The dykes represent the last known igneous event in the region, and are not metamorphosed. Including dykes in the Northampton Inlier (Fig. 1), which yield similar paleomagnetic directions and are similar in age (748 ± 8 Ma, K–Ar, Embleton and Schmidt, 1985), the swarm extends for >900 km along the western and northern margins of Western Australia, and covers an area of 180,000 km^2.

The MDS has been considered to be related to a Neoproterozoic mantle plume (Ernst and Buchan, 2001; Li et al., 2003b) or to separation of an unknown continent from Western Australia (Wingate and Giddings, 2000). However, the geochemical and isotopic characteristics of the MDS have not been documented, and petrogenesis of the dykes is not understood. Did the MDS dykes crystallise from a common parental magma? Do their geochemical and isotopic compositions indicate a close affinity to plume-derived basaltic rocks? In this paper, we present geochemical and Nd–Hf isotopic results from the MDS samples, and use these data to investigate their petrogenesis and possible genetic links with Neoproterozoic plume activity during Rodinia breakup.

2. Samples and analytical techniques

Although typically less than 30 m wide and fine- to medium-grained, some dykes are wider than 300 m and coarse-grained. Most dykes are composed of quartz dolerite or gabbro, exhibit intergranular to subophitic textures, and contain augite ± pigeonite, plagioclase, interstitial quartz and quartz-feldspar granophyre, minor magnetite and apatite. Alteration is slight to moderate, and is variable between dykes and between samples from the same dyke; plagioclase is locally sericitised, particularly along fractures, and pyroxenes are partially altered to bluish-green amphibole and chlorite. Orthopyroxene in some samples is subordinate to clinopyroxene and is partially replaced by talc, serpentine, and chlorite. Samples used for geochemistry are fractions of those collected originally for paleomagnetic study by Wingate and Giddings (2000). Consistency in paleomagnetic directions indicates that all dykes sampled are similar in age.

Sixteen samples from eight dykes were analyzed for major and trace elements at the Guangzhou Institute of Geochemistry, Chinese Academy of Sciences, and the

Table 1
Major and trace element data for the MDS dolerites

Sample #	EDMH2.2	EDMB7.2	EDMC	EDMC4.3	EDMD15.2	EDME16.2	B6	B6.1
Latitude (°S)	23.85	23.91	23.96	23.96	23.46	23.71	23.27	23.27
Longitude (°E)	115.55	115.56	115.61	115.61	115.43	115.63	115.77	115.77
Major elements (%)								
SiO_2	51.71	50.18	50.07	49.67	50.80	49.56	48.13	49.12
TiO_2	0.89	1.89	2.64	2.39	1.04	1.14	0.86	1.94
Al_2O_3	15.98	13.38	15.11	13.54	16.47	16.38	14.30	15.86
Fe_2O_3	11.14	14.73	15.21	14.80	10.73	11.42	11.56	14.10
MnO	0.15	0.20	0.19	0.19	0.15	0.16	0.15	0.18
MgO	7.67	6.77	3.35	6.30	5.82	6.48	11.95	5.03
CaO	11.60	9.94	8.74	10.01	11.34	10.88	9.01	9.54
Na_2O	1.60	2.19	2.65	2.41	2.12	2.01	1.90	2.27
K_2O	0.40	0.64	1.27	0.73	0.82	0.90	0.65	1.05
P_2O_5	0.04	0.18	0.31	0.24	0.06	0.10	0.08	0.10
LOI	0.59	0.59	1.00	0.00	0.77	1.10	0.86	1.11
Total	101.77	100.70	100.54	100.29	100.11	100.12	99.45	100.30
Mg#	0.62	0.52	0.34	0.50	0.56	0.57	0.71	0.45
Fe/Mn	66.8	66.3	72.0	70.1	64.4	64.2	69.4	66.8
Trace elements (ppm)								
Sc	31.9	33.7	28.7	37.1	28.5	30.7	21.2	29.5
V	117	267	266	307	212	211	138	360
Cr	158	179	18	181	207	272	357	83
Ni	70	119	42	80	87	154	372	76
Ga	13.0	19.2	23.3	20.9	18.2	17.1	14.1	20.5
Rb	17.3	17.6	40.6	22.7	30.0	32.0	32.6	47.3
Sr	167	201	214	289	231	195	164	212
Y	15.1	25.8	39.0	28.1	13.6	17.9	11.7	19.4
Zr	100	154	246	181	68.1	98.5	70.1	108
Nb	6.55	18.5	24.9	20.6	7.67	10.6	5.64	13.0
Ba	91	130	286	157	123	146	87	169
La	10.2	15.4	27.7	16.4	9.3	13.2	8.8	13.8
Ce	22.8	36.2	62.8	38.7	20.5	29.2	19.8	30.7
Pr	3.02	5.08	8.70	5.45	2.73	3.93	2.58	4.10
Nd	12.1	21.2	34.7	23.0	10.9	15.4	10.2	16.2
Sm	2.77	5.07	7.88	5.36	2.45	3.39	2.26	3.58
Eu	0.95	1.64	2.33	1.88	1.16	1.11	0.76	1.32
Gd	3.02	5.54	8.26	5.82	2.67	3.80	2.36	3.78
Tb	0.51	0.92	1.36	0.96	0.44	0.61	0.39	0.65
Dy	2.96	5.11	7.74	5.45	2.64	3.43	2.22	3.74
Ho	0.59	1.00	1.49	1.04	0.51	0.70	0.45	0.74
Er	1.59	2.62	3.98	2.75	1.39	1.89	1.19	2.01
Tm	0.24	0.39	0.58	0.41	0.21	0.29	0.18	0.30
Yb	1.54	2.48	3.73	2.58	1.34	1.90	1.13	1.95
Lu	0.25	0.40	0.57	0.40	0.22	0.30	0.18	0.31
Hf	2.38	4.17	6.41	4.44	1.89	2.70	1.85	2.93
Ta	0.38	1.12	1.42	1.21	0.45	0.62	0.35	0.76
Th	2.92	2.87	6.09	2.72	2.47	3.83	3.02	3.79
U	0.40	0.50	1.05	0.54	0.47	0.72	0.70	0.75

Sample #	EDMI1.1	EDMI4.1	B7	EDMG	EDME3.2	EDMH1.2	EDMF	EDMF1.2
Latitude (°S)	23.83	23.83	23.83	23.88	23.71	23.85	23.81	23.81
Longitude (°E)	115.88	115.88	115.88	115.64	115.63	115.55	115.67	115.67
Major elements (%)								
SiO_2	49.19	51.01	50.87	50.06	49.38	50.52	49.13	47.49
TiO_2	1.31	1.16	1.06	2.07	2.20	1.04	2.82	3.06
Al_2O_3	14.54	14.92	14.54	14.65	13.85	16.52	13.66	12.80

Table 1 (*Continued*)

Sample #	EDMI1.1	EDMI4.1	B7	EDMG	EDME3.2	EDMH1.2	EDMF	EDMF1.2
Fe_2O_3	11.80	12.28	11.57	13.83	14.75	11.12	15.80	17.25
MnO	0.17	0.16	0.17	0.18	0.19	0.16	0.21	0.21
MgO	6.80	6.60	7.32	5.07	5.63	7.11	4.69	5.58
CaO	10.65	10.20	10.70	9.00	9.33	11.34	8.44	9.08
Na_2O	1.93	1.79	1.85	2.33	2.27	1.99	2.39	2.23
K_2O	1.01	0.98	0.80	1.13	1.18	0.54	1.42	1.03
P_2O_5	0.08	0.09	0.09	0.21	0.23	0.08	0.49	0.40
LOI	1.77	1.30	1.49	1.19	1.39	0.53	0.80	0.85
Total	99.25	100.50	100.45	99.73	100.40	100.92	99.85	99.99
Mg#	0.57	0.56	0.60	0.46	0.47	0.60	0.41	0.43
Fe/Mn	62.5	69.1	61.3	69.2	69.9	62.6	67.7	73.9
Trace elements (ppm)								
Sc	34.7	35.9	33.0	29.5	33.6	32.4	30.1	33.8
V	239	237	191	279	295	192	255	319
Cr	214	171	266	93	119	191	116	135
Ni	109	88	101	84	89	99	87	88
Ga	17.9	18.1	16.8	21.1	21.1	17.1	23.3	21.7
Rb	57.9	56.9	45.2	43.1	51.3	18.6	50.5	35.3
Sr	187	177	179	259	271	202	283	256
Y	18.1	17.3	17.2	28.9	29.5	14.5	43.3	37.1
Zr	100	90.5	94.3	174	174	78.3	300	249
Nb	12.1	9.99	9.01	20.2	19.7	8.48	30.1	31.9
Ba	160	145	114	219	494	109	314	202
La	12.5	11.6	11.7	20.5	19.4	9.8	32.4	25.2
Ce	28.2	25.8	26.6	46.5	45.0	22.0	73.9	58.6
Pr	3.73	3.45	3.52	6.34	6.19	2.96	10.5	8.37
Nd	14.8	13.9	14.2	25.7	25.6	11.8	42.8	34.8
Sm	3.37	3.11	3.20	5.77	5.81	2.63	9.48	7.91
Eu	1.06	1.05	1.07	1.79	1.86	0.93	2.86	2.46
Gd	3.55	3.35	3.47	6.25	6.41	2.88	9.77	8.30
Tb	0.61	0.57	0.58	1.02	1.03	0.48	1.59	1.35
Dy	3.42	3.23	3.35	5.69	5.80	2.78	8.69	7.35
Ho	0.68	0.64	0.67	1.13	1.14	0.55	1.66	1.41
Er	1.82	1.74	1.79	2.97	3.00	1.49	4.35	3.62
Tm	0.27	0.26	0.27	0.44	0.45	0.22	0.63	0.52
Yb	1.76	1.69	1.79	2.86	2.85	1.42	4.02	3.33
Lu	0.28	0.27	0.29	0.45	0.44	0.23	0.62	0.51
Hf	2.60	2.34	2.54	4.76	4.57	2.02	7.76	6.27
Ta	0.72	0.57	0.55	1.25	1.14	0.50	1.71	1.87
Th	3.38	3.10	3.16	5.15	4.29	2.53	6.27	4.42
U	0.63	0.57	0.62	0.89	0.77	0.53	1.12	0.78

Sample#	International standard rock					
	AGV-1 1st	AGV-1 2nd	AGV-1 Govindaraju (1994)	BHVO-2 1st	BHVO-2 2nd	BHVO-2 Gao et al. (2002)
Major elements (%)						
SiO_2	58.97	59.23	58.84	49.98	49.64	49.90
TiO_2	1.04	1.07	1.05	2.70	2.73	2.73
Al_2O_3	16.96	17.12	17.15	13.74	13.28	13.50
Fe_2O_3	6.64	6.76	6.77	12.45	12.35	12.30
MnO	0.10	0.10	0.09	0.17	0.17	0.17
MgO	1.50	1.55	1.53	7.25	7.30	7.23
CaO	4.79	4.81	4.94	11.53	11.35	11.40
Na_2O	4.16	4.20	4.26	0.52	0.51	0.52
K_2O	2.86	2.88	2.92	2.32	2.21	2.22
P_2O_5	0.48	0.50	0.49	0.28	0.27	0.27
LOI						

Table 1 (*Continued*)

Sample#	International standard rock					
Total						
Mg#						
Fe/Mn						
Trace elements (ppm)						
Sc	11.9	12.0	12.2	28.4	33.3	31
V	121	122	121	299	410	329
Cr	10.7	10.3	10.1	281	269	285
Ni	15.9	15.0	16.0	118	127	112
Ga	20.4	20.0	20.0	20.8	21.2	21
Rb	68.2	68.5	67.3	9.40	10.1	10.1
Sr	652	657	662	365	413	382
Y	19.8	20.7	20.0	24.5	24.7	23
Zr	227	226	227	162	165	160
Nb	14.6	14.5	15.0	17.1	17.6	16.4
Ba	1185	1168	1226	127	140	137
La	38.5	38.4	38.0	14.5	16.1	15.6
Ce	68.9	68.6	67.0	36.5	39.6	37
Pr	8.74	8.99	7.60	5.13	4.78	5.0
Nd	32.7	31.9	33.0	24.4	24.7	24
Sm	5.79	5.75	5.90	6.04	6.39	5.8
Eu	1.61	1.60	1.64	2.09	2.17	2.0
Gd	4.88	4.93	5.00	6.07	5.95	5.9
Tb	0.67	0.69	0.70	0.93	0.94	0.86
Dy	3.66	3.65	3.60	5.15	5.18	4.9
Ho	0.69	0.69	0.67	0.95	0.94	0.91
Er	1.84	1.76	1.70	2.30	2.44	2.3
Tm	0.33	0.34	0.34	0.30	0.31	0.30
Yb	1.70	1.73	1.72	1.91	1.99	2.0
Lu	0.25	0.27	0.27	0.27	0.29	0.26
Hf	5.15	5.21	5.10	4.17	4.04	4.1
Ta	0.93	0.95	0.90	1.19	1.20	0.94
Th	6.34	6.30	6.50	1.39	1.41	1.18
U	1.92	1.91	1.92	0.51	0.51	0.44

Mg# = $Mg/(Mg + Fe^{2+})$, assuming $Fe_2O_3/(FeO + Fe_2O_3) = 0.20$. Total iron as Fe_2O_3.

data are listed in Table 1. Major element oxides were determined by standard X-ray fluorescence (XRF). Samples were prepared as glass discs using a Rigaku desktop fusion machine, formed by mixing 0.50 g of rock powder (dried at 110 °C) with 4.0 g of lithium tetraborate for 15 min at 1100 °C in 95%Pt–5%Au crucibles. Analyses were performed on a Rigaku ZSX100e instrument. Calibration lines used in quantification were produced by bivariate regression of data from 36 reference materials encompassing a wide range of silicate compositions (Li et al., 2005a). Calibrations incorporated matrix corrections based on the empirical Traill–Lachance procedure, and analytical uncertainties are between 1 and 5%. A loss-on-ignition (LOI) measurement was undertaken on samples of dried rock powder by heating in a pre-ignition silica crucible to 1000 °C for 1 h and recording the percentage weight loss.

Trace elements were analyzed by inductively coupled plasma mass spectrometry (ICP-MS), using a Perkin-Elmer Sciex ELAN 6000 instrument. Analytical procedures are similar to those described by Li (1997). About 50 mg of each powdered sample was dissolved in a high-pressure Teflon bomb for 24 h using a HF + HNO_3 mixture. Rh was used as an internal standard to monitor signal drift during counting. The USGS and Chinese National standards BCR-1, BHVO-1, W-2 and GSR-3 were chosen for calibrating element concentrations of measured samples. Analytical precision is typically 2–5%. Other two USGS rock standards AGV-1 and BHVO-2 were analyzed as unknowns for data quality control. Replicate analyses of the standard rocks are in good agreement with the reference values (Table 1).

Nd isotopic compositions were determined using a Micromass Isoprobe multi-collector ICP-MS at the

Guangzhou Institute of Geochemistry, using analytical procedures described by Li et al. (2004a). Nd fractions were separated by passing through cation columns followed by HDEHP columns, and the aqueous sample solution was taken up in 2% HNO_3 and introduced into the MC-ICP-MS using a Meinhard glass nebuliser with an uptake rate of 0.1 ml/min. The inlet system was cleaned for 5 min between analyses using high-purity 5% HNO_3 followed by a blank solution of 2% HNO_3. Measured $^{143}Nd/^{144}Nd$ ratios were normalised to $^{146}Nd/^{144}Nd = 0.7219$, and the reported $^{143}Nd/^{144}Nd$ ratios were further adjusted relative to the Shin Etsu JNdi-1 standard of 0.512115, corresponding to the La Jolla standard of 0.511860 (Tanaka et al., 2000).

For Hf isotopic analysis, about 100 mg rock powder and 200 mg $Li_2B_4O_7$ were mixed homogeneously. The mixture was digested for 15 min at 1200 °C in Pt–Au crucibles, then dissolved in 2 M HCl. Hf fraction was separated by using a modified single-column separation procedure by ion exchange using Eichrom® Ln-Spec resin (Li et al., 2005b). The sample was loaded in 2 M HCl. Purification of Hf were achieved using 3 M HCl to elute the matrix elements and REE, 6 M HCl to elute Lu, 4 M HCl with 0.4‰ H_2O_2 to elute Ti, and 1 M HCl with 0.04 M HF to elute Nb and Ta. Finally, Hf was collected using 1 M HCl with 0.2 M HF. Hf isotopes were determined using a Finnigan Neptune MC-ICP-MS at the Institute of Geology and Geophysics Chinese Academy of Sciences. The measured $^{176}Hf/^{177}Hf$ ratios were normalised to $^{179}Hf/^{177}Hf = 0.7325$, and the reported $^{176}Hf/^{177}Hf$ ratios were further adjusted relative to the JMC 475 standard of 0.282160 (Nowell et al., 1998).

Nd and Hf isotopic data are listed in Table 2. The $^{143}Nd/^{144}Nd$ and $^{176}Hf/^{177}Hf$ ratios of the USGS basalt standards BCR-1 and BHVO-1 measured during this study are also presented in Table 2. Our results are in good agreement with the reported values (Raczek et al., 2003; Lapen et al., 2004).

3. Results

The MDS samples are characterised by low total alkalis ($Na_2O + K_2O < 3.5\%$) over a range of SiO_2 = 47–51%, plotting within the sub-alkaline basalt field on a total alkalis versus silica plot (Fig. 2a). They have tholeiitic compositions in terms of exhibiting a typical tholeiitic trend in an AFM diagram (Fig. 2b) and high FeO_T/MgO ratio that increases with increasing TiO_2 (not shown). Apart from the olivine gabbro sample B6 having high Mg# = 0.71 owing to clinopyroxene accumulation, all others range from moderate to highly evolved compositions with Mg# between 0.62 and 0.34, coupled with low Ni (18–154 ppm) content, as a result of extensive fractional crystallization. In the Harker diagram (Fig. 3), dolerites show relatively constant Al_2O_3, decrease of CaO, Fe_2O_3, Ni and Cr, and increase of TiO_2, K_2O and Na_2O with decreasing Mg#, indicating fractional crystallization of predominant olivine and clinopyroxene, but not Ti–Fe oxides.

Although the MDS dolerites have variable REE abundance with La_N = 37–137 as a result of high degrees of fractionation, they all exhibit uniform chondrite-normalised LREE-enriched patterns with relatively constant La_N/Sm_N = 2.1–2.5 (Fig. 4). Apart from samples EDMHB6-1 and EDME15.2 showing clear Eu positive anomaly ($Eu/Eu^* = 1.1–1.3$) due to plagioclase accumulation, all others have slightly negative to insignificant Eu anomalies ($Eu/Eu^* = 0.88–1.03$). Normalised to primitive mantle, the dolerite samples show increasing enrichment in incompatible trace elements between Lu and Th (with increasing incompatibility) except for weak negative anomalies in Nb and Ta (Fig. 5).

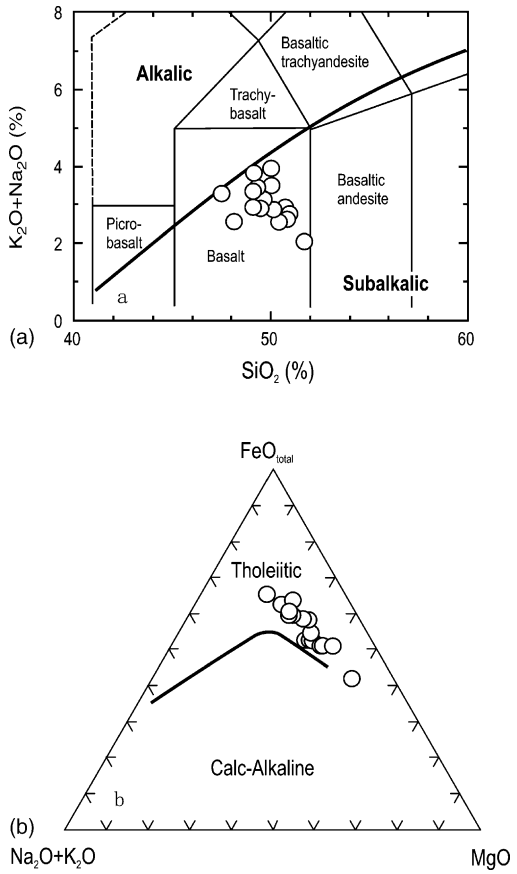

Fig. 2. (a) Total alkalis vs. SiO_2 diagram for classification of the Mundine Well dolerites and (b) whole-rock alkali ($Na_2O + K_2O$)–FeO_T–MgO (AFM) plots.

Table 2
Sm–Nd and Lu–Hf isotopic data for the MDS dolerites

Sample#	$^{147}Sm/^{144}Nd$	$^{143}Nd/^{144}Nd$	$\pm2\sigma_m$	$\varepsilon Nd(T)$	$^{176}Lu/^{177}Hf$	$^{176}Hf/^{177}Hf$	$\pm2\sigma_m$	$\varepsilon Hf(T)$
EDMH2.2	0.138	0.512250	0.000012	−1.91	0.0149	0.282539	0.000008	0.93
EDMB7.2	0.144	0.512427	0.000013	0.94	0.0136	0.282588	0.000006	3.32
EDMC	0.137	0.512328	0.000012	−0.29	0.0126	0.282557	0.000007	2.73
EDMC4.3	0.141	0.512428	0.000013	1.28	0.0128	0.282639	0.000006	5.54
EDMD15.2	0.136	0.512177	0.000012	−3.15	0.0165	0.282511	0.000011	−0.87
EDME16.2	0.133	0.512204	0.000009	−2.30	0.0158	0.282504	0.000006	−0.74
B6	0.133	0.512217	0.000011	−2.09	0.0138	0.282517	0.000010	0.71
B6.1	0.134	0.512204	0.000009	−2.38	0.0150	0.282540	0.000010	0.92
EDMI1.1	0.138	0.512194	0.000013	−2.96	0.0153	0.282528	0.000007	0.37
EDMI4.1	0.136	0.512253	0.000014	−1.60	0.0164	0.282540	0.000009	0.22
B7	0.136	0.512211	0.000013	−2.44	0.0162	0.282532	0.000008	0.02
EDMG	0.136	0.512277	0.000011	−1.10	0.0134	0.282534	0.000007	1.52
EDME3.2	0.137	0.512344	0.000010	0.02	0.0137	0.282562	0.000004	2.37
EDMH1.2	0.134	0.512237	0.000012	−1.80	0.0162	0.282538	0.000007	0.28
EDMF	0.134	0.512341	0.000012	0.26	0.0113	0.282552	0.000020	3.20
EDMF1.2	0.137	0.512451	0.000013	2.11	0.0115	0.282628	0.000008	5.78
International standard rock								
BCR-1		0.512645	0.000010			0.282883	0.000010	
BHVO-1		0.512953	0.000009			0.283102	0.000009	

T = 755 Ma, crystallization age of the MDS dolerites (Wingate and Giddings, 2000).

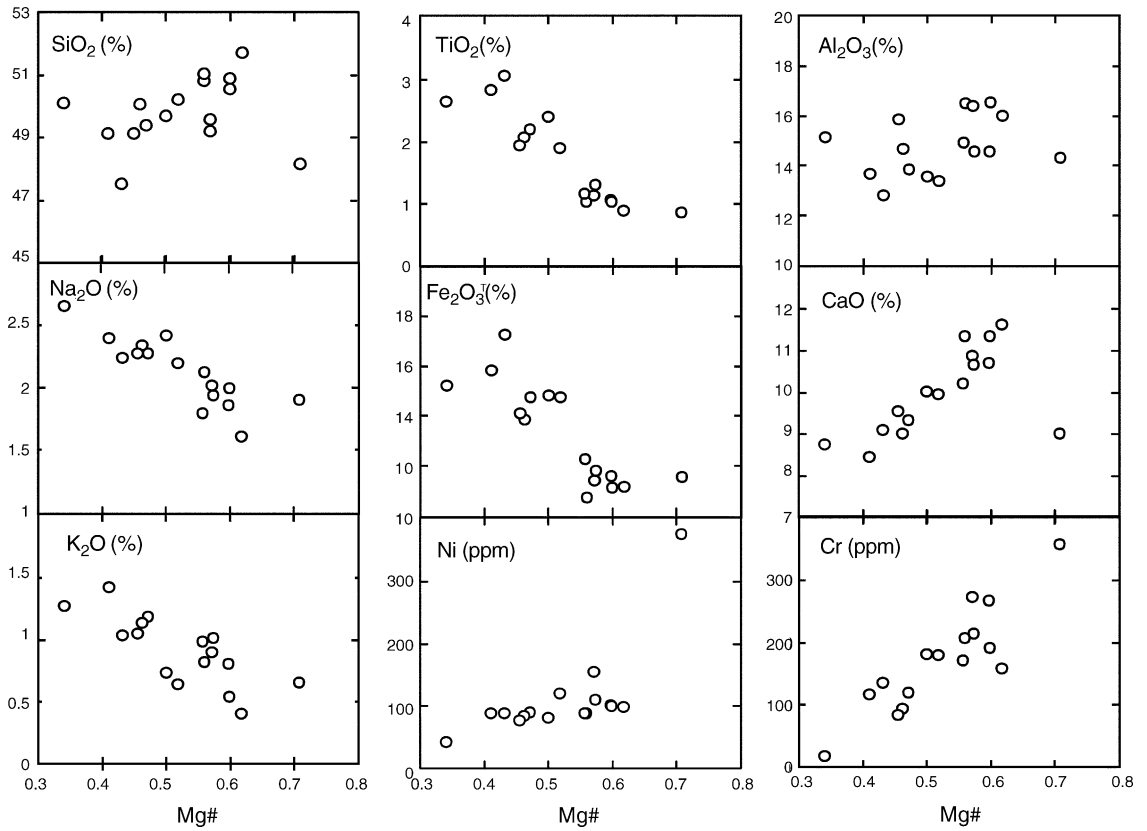

Fig. 3. Harker variation diagram for the MDS dolerites.

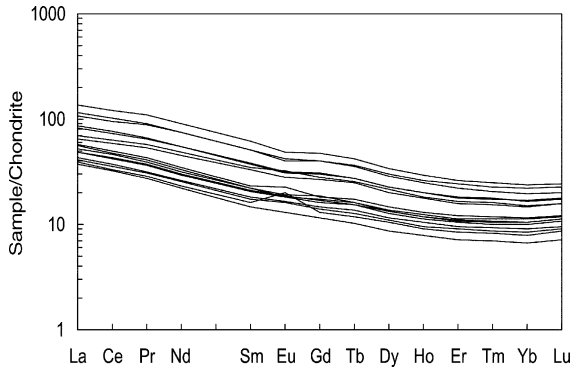

Fig. 4. Chondrite-normalised REE patterns for the MDS dolerites. Normalising values from Sun and McDonough (1989).

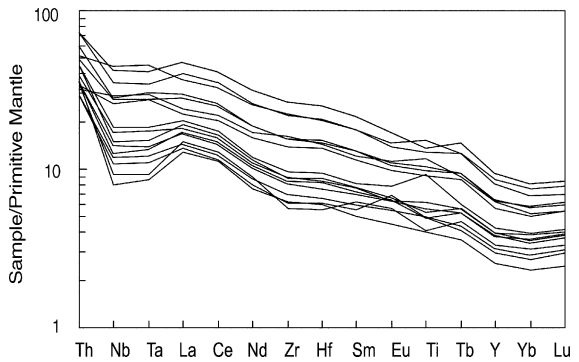

Fig. 5. Primitive mantle-normalised incompatible trace element spidergrams for the MDS dolerites. Normalising values from Sun and McDonough (1989).

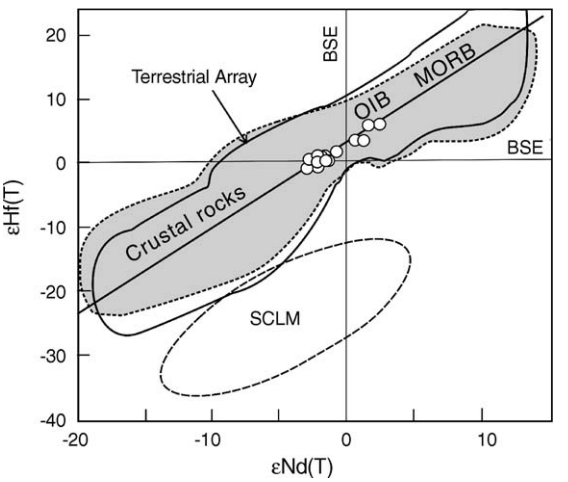

Fig. 6. Plot of εHf(T) vs. εNd(T) values for the MDS dolerites. "Terrestrial Array" indicates the Hf–Nd isotopic variation of present-day OIB, MORB and crustal clastic sediments and felsic igneous rocks (Vervoort et al., 1999); the grey area shows the time-corrected "Terrestrial Array" at ca. 0.76 Ga; the estimated Hf–Nd isotope range for the subcontinental lithosphere mantle is after Griffin et al. (2000). SCLM: subcontinental lithospheric mantle; BSE: bull silicate earth.

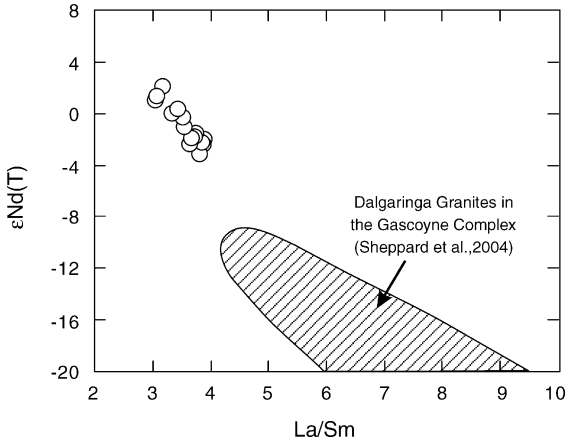

Fig. 7. Plot of La/Sm vs. εNd(T) value for the MDS dolerites. Data for the Dalgaringa granite, one of the main wall-rocks of the MDS dolerites, in the Gascoyne Complex are from Sheppard et al. (2004).

The MDS dolerites have fairly constant $^{147}Sm/^{144}Nd$ ratios between 0.133 and 0.144, but relatively variable $^{144}Nd/^{144}Nd$ ratios ranging from 0.51218 to 0.51245. The calculated initial εNd(T) values range from −3.15 to 2.11 (Table 2). Their $^{176}Lu/^{177}Hf$ ratios range from 0.0113 to 0.0164. The measured $^{176}Hf/^{177}Hf$ ratios are between 0.28251 and 0.28264, corresponding to initial εHf(T) values of −0.87 to 5.78 (Table 2). There is a positive correlation between εHf(T) and εNd(T) values (Fig. 6), indicative of involvement of two major components in their origin. The εNd(T) values are correlated negatively with La/Sm ratios (Fig. 7), trending towards the field of Gascoyne Complex granite (Sheppard et al., 2004). Thus, the parental magma of the MSD dolerites was likely originated from a time-integrated depleted mantle source with varying degrees of crustal contamination.

4. Petrogenesis

Based on data presented here, most major and trace element variations are coherent and consistent with derivation of the MDS from a common parental magma. In the Pearce element ratio plots of Si/K versus 0.5[(Mg + Fe) + 1.5Ca]/K and (2Ca + 3Na)/K (Fig. 8), the MDS dolerites yield tight linear regression lines with slopes of 0.5899 and 0.5936, respectively, indicating that these samples could have been derived from a common parental magma by crystal separation/addition of a three-phase assemblage of olivine, clinopyroxene and plagioclase (Russell and Nicholls, 1988). This result is consistent with MDS dolerite petrography and major and trace element characteristics.

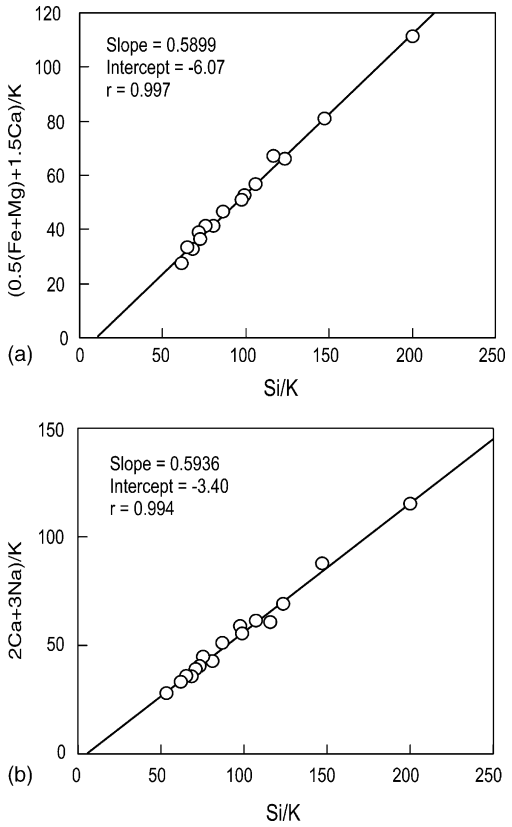

Fig. 8. Pearce element ratio diagram of (a) [0.5(Mg + Fe) + 1.5Ca]/K vs. Si/K and (b) (2Ca + 3Na)/K vs. Si/K for the MDS dolerites. Slopes of <1 for two regression lines indicate derivation of MDS samples from a common parental magma by crystal separation/addition of olivine, clinopyroxene, and plagioclase. Correlation coefficients (R) are 0.997 and 0.994 for plots (a) and (b), respectively.

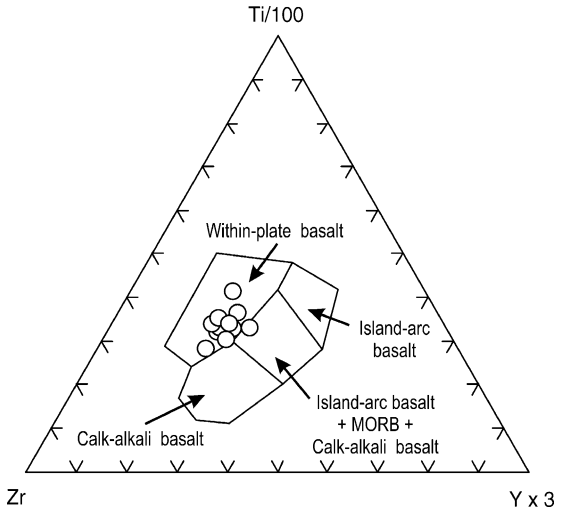

Fig. 9. Ti–Zr–Y discrimination diagram of Pearce and Cann (1973). All the MDS dolerites plot within the field of within-plate basalt.

The MDS samples exhibit characteristic incompatible trace element patterns similar to those of intraplate basalts, rather than volcanic arc basalts, and plot mainly within the intraplate basalt field in discrimination diagrams (Pearce and Cann, 1973) (Fig. 9). However, the samples also exhibit elevated La/Sm, Th and relatively nonradiogenic Nd isotopic compositions, which are different from those commonly observed in oceanic island basalts (OIB) such as the Hawaii basalts (Huang and Frey, 2003; Rhodes and Vollinger, 2004), but similar to many continental flood basalts (CFB) (Hawkesworth et al., 1986, 1995; Mahoney, 1988; Carlson, 1991; Hergt et al., 1991).

Origin and petrogenesis of the CFB have been a long-standing issue of debate. A central problem is that many CFB, particularly those typical low-Ti CFB, are characterised by enrichment of incompatible elements, negative Ta–Nb–Ti anomalies, high $^{87}Sr/^{86}Sr$ and low $^{143}Nd/^{144}Nd$. These characteristics could either be inherited from the metasomatized subcontinental lithosphere mantle (SCLM), or reflect addition of granitic materials from the continental crust. It is noted that significant partial melting within the continental lithosphere mantle, the coldest part of the mantle, will not occur unless its solidus is depressed by presence of volatiles during plume–lithosphere interaction (Gallagher and Hawkesworth, 1992). Evaluation of the volatile content in the source of CFB, however, is difficult. Thus, geochemical variations are commonly used to constrain the nature of end-member components involved in the CFB (e.g., Hawkesworth et al., 1995; Kieffer et al., 2004).

It is noteworthy that no correlation between SiO_2, Al_2O_3, and MgO or Mg# exist in the MDS dolerites (Fig. 3), because they underwent crystal separation/addition of a three-phase assemblage of olivine, clinopyroxene and plagioclase. Consequently, SiO_2 is not correlated with MgO and $\varepsilon Nd(T)$ values, indicating that the major elements are inappropriate for constraining the end-member components. However, the minor and trace elements, particularly these element ratios, will give a robust estimation of the end-member components (e.g., Hawkesworth et al., 1995).

Fig. 10 shows that Th/La of the MDS dolerite is correlated positively with La/Sm and negatively with Nb/U, Nb/La and Nb/Th. The average compositions of Archean upper crust (Taylor and McLennan, 1985) and primitive continental arc basalt (Kelemen et al., 2004) are also shown for reference. Despite highly variable compositions of metasomatized SCLM, many studies demonstrated that metasomatized lithospheric peridotites, particularly those that interacted with carbonate-rich fluids,

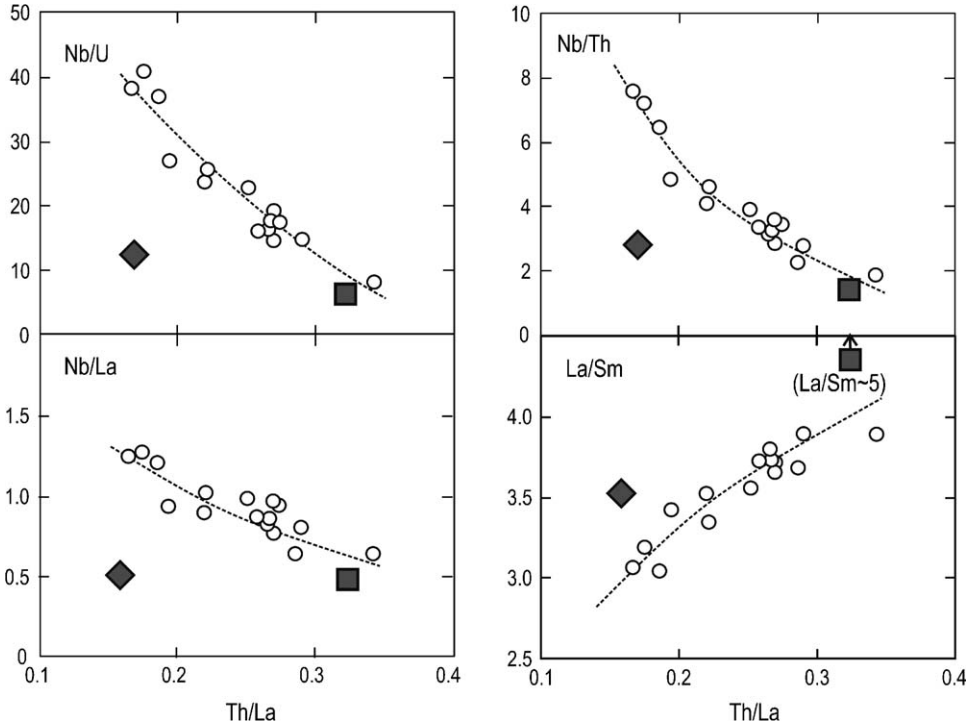

Fig. 10. Variations of Nb/U, Nb/Th, Nb/La, and La/Sm with Th/La for the MDS dolerites. Large filled square and diamond represent the average compositions of Archean upper crust (Taylor and McLennan, 1985) and primitive continental arc basalt (Kelemen et al., 2004), respectively.

have characteristically high ratios of REE to HFSE (e.g., Baker et al., 1998; Xu et al., 2003). In their mantle-normalised trace element spidergrams, these metasomatized peridotites are characterized by significant negative Nb (Ta), Zr (Hf) and Ti anomalies, resembling those of the arc basalt. Compared with the primitive continental arc basalt, the MDS dolerites have significantly higher Nb/U, Nb/La and Nb/Th ratios and lower La/Sm at comparable Th/La ratio of ~0.17. The arc basalt deviates clearly from the geochemical trends of the MDS dolerites, indicating that the latter was unlikely derived from a metasomatized SCLM source. On the other hand, the average composition of Archean upper crust, apart from La/Sm, follows the geochemical trends of the MDS dolerites well, suggesting that geochemical variation of the MDS dolerites is most likely due to crustal contamination. This interpretation is consistent with field observations that several dykes are contaminated extensively by granitic xenoliths and some have metamorphosed and partially remelted their granitoid wall-rocks (Wingate and Giddings, 2000).

On the Hf–Nd isotopic plot, the MDS dolerites display εHf and εNd values significantly higher than the SCLM field (Griffin et al., 2000). Instead, they plot along the "Terrestrial Array" that extends from MORB through OIB to continental crust (Vervoort et al., 1999) (Fig. 6). Therefore, Hf–Nd isotopic variations clearly support the interpretation that the MDS dolerites were derived from an asthenospheric mantle source, rather than SCLM, but with crustal contamination.

We notice that the MDS dolerites have Fe/Mn ratio = 61–74, which is positively correlated with εNd(T) value (Fig. 11). Amongst the basalts formed in distinct settings, most MORB have Fe/Mn ratio around 55–59, comparable with Fe/Mn = 54–59 of island arc

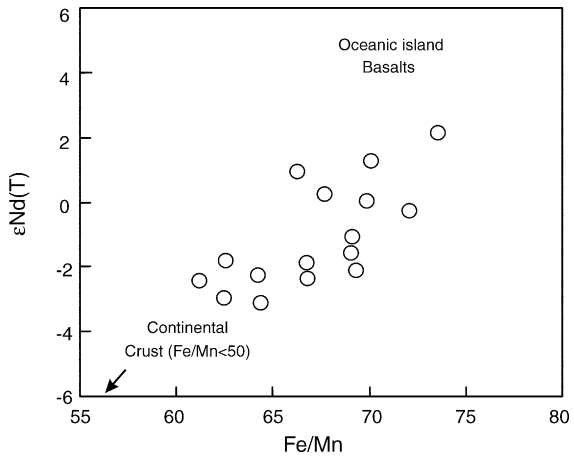

Fig. 11. Plot of εNd(T) value vs. Fe/Mn ratio for the MDS dolerites.

basalts, whereas OIB usually have Fe/Mn > 60 (Wilson, 1989). Mantle peridotites and Archean upper crust have Fe/Mn ratio of ~60 (McDonough and Sun, 1995) and ~44 (Taylor and McLennan, 1985), respectively. Precise Fe/Mn measurements indicate that the Hawaiian OIB have Fe/Mn ratio = 65–71, whereas the MORB have Fe/Mn = 55–58 (Humayun et al., 2004). Although the genesis of excess Fe in the Hawaiian OIB is controversial (Humayun et al., 2004; Lee, 2004), it seems that high Fe/Mn is characteristic of the plume-derived magmas. The MDS dolerites have Fe/Mn ratio comparable with those of the Hawaiian OIB, indicating their affinity to plume-derived magma. Their positive correlation between Fe/Mn and $\varepsilon Nd(T)$ value is consistent with crustal contamination of an OIB-like basaltic magma.

Owing to crustal contamination, the geochemical and isotopic compositions of the MDS dolerites, even the least-contaminated samples, are not reflective of their mantle source. Assuming the uncontaminated, parental magma of the dolerites to have a Th/La ratio of ~0.1, similar to the typical OIB (Sun and McDonough, 1989), extrapolations from the geochemical correlations yield estimates of Nb/U ≈ 50, Nb/La ≈ 1.5, Nb/Th ≈ 15, La/Sm ≈ 2.5, $\varepsilon Nd(T) \approx 5$ and $\varepsilon Hf(T) \approx 9$ for the parental magma. All these values are typical of OIB. The major element composition of the parental magma can be calculated by stripping off the chemical effects of crustal contamination and fractional crystallization. This was done using a numerical procedure. To minimize the chemical effects of crustal contamination and consider the olivine crystallization only, we started the calculation with two least-contaminated, less-fractionated samples B7.2 and C4.3 (Nb/La > 1, $\varepsilon Nd(T) > 0$, and MgO > 6%). Equilibrium olivine is added at 1% increments until the resulting basaltic magma is in equilibrium with Fo_{89} olivine, using $Kd = (FeO/MgO)^{Ol}/(FeO/MgO)^{L} = 0.3$ (Roeder and Emslie, 1970) and assuming Fe^{2+}/total Fe = 0.85. This method is valid for basalts having MgO > 6% (McKenzie and O'Nions, 1991). After removing effect of 40% olivine crystallization, the result is a picritic magma containing about 20% MgO. Thus, the MDS dolerites were most likely derived from an anomalously hot, OIB-type mantle plume source with varying degrees of crustal contamination during magma ascent and emplacement.

5. Neoproterozoic mantle plume events during Rodinia breakup

Dykes similar in age to the 755 Ma MDS dolerites in northwestern Australia also occur in Seychelles and in South China. The Seychelles dolerites (Tucker et al., 2001; Ashwal et al., 2002), dated at 750 ± 3 Ma, were mingled with coeval granitoids which have long been considered by most workers as being formed in a rift- or plume-related extensional tectonic setting (Weis and Deutsch, 1984; Plummer, 1995; Stephens et al., 1997; Bowden et al., 2001), except for Ashwal et al. (2002) who recently re-interpreted them as reflecting Andean-type arc magmatism. The Seychelles dolerites have tholeiitic compositions (Ashwal et al., 2002), and are characterised by high TiO_2 (mostly 1.8–2.9%), Zr (mostly 170–220 ppm), Ti/V (50–90), and "humped" trace element spidergrams (Fig. 12), resembling OIB. They have variable $\varepsilon Nd(T)$ values of −0.9 to 5.4 and pronounced Nb and Ta negative anomalies, suggesting involvement of an Archean silicic contaminant (Ashwal et al., 2002), or, more likely, relatively young arc-crustal components. Thus, the Seychelles bimodal magmatic rocks most likely formed in a non-orogenic regime as proposed by most previous workers, despite the possible location of the Seychelles at the periphery of the Rodinia supercontinent (Torsvik et al., 2001).

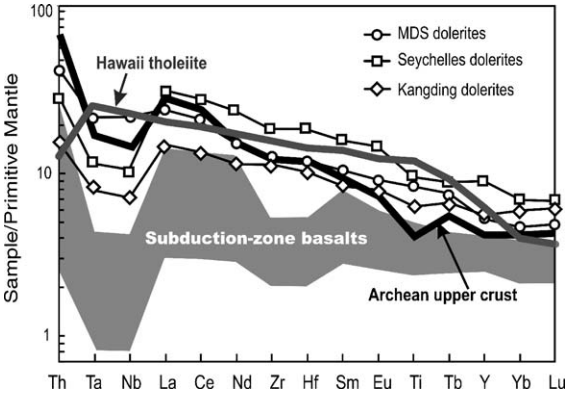

Fig. 12. Comparison of primitive mantle-normalised incompatible trace element spidergrams for the ca. 755–700 Ma dolerites from Seychelles (Ashwal et al., 2002), western Yangtze Craton (Li et al., 2003b), and MDS dolerites (this study). They exhibit consistent OIB-like patterns, apart from elevated Th and varying degrees of Nb and Ta depletion due to addition of continental and/or arc crust components. Data for the average Archean upper crust (UC) are from Taylor and McLennan (1985), and average Hawaii tholeiites from Huang and Frey (2003). The shade area is the range for the subduction zone basalts, with the lower and upper limit being defined by "average" low-K and high-K basalts, respectively (Tatsumi and Eggins, 1995).

Abundant dolerite dykes occur within the Kangdian Rift along the western margin of the Yangtze craton in South China (Li et al., 2003b). Although precise isotopic ages have not been determined directly for the Kangdian dolerites, field observations that mafic and felsic magmas intermingled with each other implies that the dykes are the same age as the surrounding granites, which are dated at 755 ± 6 Ma (Li et al., 2003b). The Kangdian

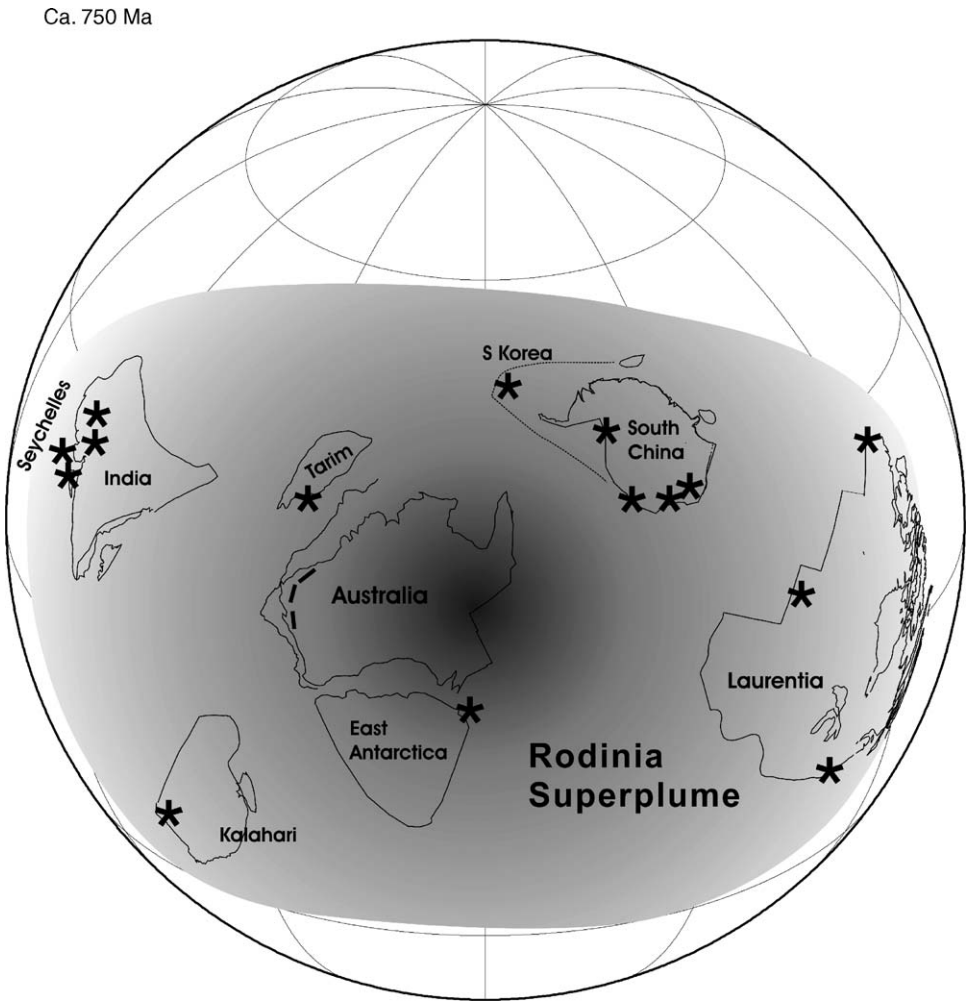

Fig. 13. A schematic diagram illustrating the broken-up Rodinia supercontinent above the Rodinia superplume at ca. 750 Ma (modified after Li et al., 2003b, 2004b). Locations of ca. 750 Ma igneous activities discussed in the text are shown as asterisks.

dolerites are also tholeiitic in composition, with geochemical characteristics of intraplate basalts (Fig. 12). They exhibit variably positive $\varepsilon Nd(T)$ values of 0.9–3.4 with subtle to significant Nb–Ta negative anomalies owing to varying degrees of crustal contamination. The least-contaminated sample (01KD11) displays a trace element pattern very similar to those of intraplate tholeiites of mantle plume origin (Li et al., 2003b).

Collectively, the isotopic ages, geochemical characteristics, and inferred petrogenesis, are strikingly similar for dolerite dyke suites in northwestern Australia, South China, and the Seychelles. All three suites could have been generated by melting of an asthenospheric mantle plume (or plumes) at 750–755 Ma.

Widespread, similar-aged intraplate magmatism in other continents may also be explained by plume activities. For example, extensive non-orogenic felsic igneous rocks of the Malani Igneous Suite (MIS) of Rajasthan in northwestern India, which is the world's third largest felsic magmatic province (Bhushan, 2000), were emplaced at 751–771 Ma (unpublished data of Tucker et al., cited by Torsvik et al., 2001). Alkaline bimodal igneous rocks, dated at ca. 750 Ma, are prevalent in South Korea, and are thought to have been generated in a continental rift related to the breakup of Rodinia (Lee et al., 1998, 2003). In the Kangding Rift of western South China, a number of gabbros and granites were recently dated at 764–746 Ma by SHRIMP U–Pb zircon technique (Zhou et al., 2002; Li et al., 2003b). Although these granites show some arc-like geochemical signatures (Zhou et al., 2002), they are younger than the ca. 800 Ma syn-rifting alkaline volcanic rocks (Li et al., 2002, 2005b) and coeval with the ca. 755 Ma plume-related dolerites and rift magmatism in South China (Li et al., 2003b).

Thus, they are more likely to have resulted from extensive crustal anatexis caused by conductive heating above a mantle plume, similar to the petrogenesis of those ca. 820–825 Ma granitoids in South China (Li et al., 2003a). Similar-aged syn-rifting volcanic rocks, granites and mafic intrusions also occurred in the Tarim block of northwestern China (Xu et al., 2005) and Tasmania of Australia (Li et al., 2003b; Holm et al., 2003).

In western Laurentia, ca. 750 Ma magmatic rocks occurred along rift margins, including the 740 ± 36 Ma Mount Copeland syenite gneiss (Parrish and Scammell, 1988) and the 741 ± 22 Ma Malton gneissic granite (Evenchick et al., 1984) in the southern Rocky Mountains. There were also the 751 ± 26 Ma Mount Harper Group rhyolite of northwest Canada (Roots and Parrish, 1988) and the 762 ± 44 Ma Huckleberry Formation volcanics of northern Washington (Devlin et al., 1988) at the basal parts of the rift successions (e.g., Rainbird et al., 1996). Contemporaneous bimodal rift-related igneous rocks are also documented in southeastern Laurentia, represented by 765 ± 7 Ma alkali granites, 742 ± 2 Ma metarhyolites (Fetter and Goldberg, 1995), and 741 ± 3 Ma bimodal intrusive rocks (Su, 1994) in the Blue Range province of southern Appalachians, and by 758 ± 12 Ma bimodal rift volcanics in Mount Rogers of Virginia (Aleinikoff et al., 1995). These magmatic activities are considered as plume origin and being linked to the breakup of Rodinia and the breakout of Laurentia as a relatively discrete land mass (Fetter and Goldberg, 1995).

In southern Africa, 741 ± 6 Ma rhyolites were reported in the Rosh Pinah Formation of the Gariep Belt in southwestern Namibia (Frimmel et al., 1996). They are clearly related to continental rift caused possibly by mantle plume (Frimmel et al., 2001).

It is noteworthy that all major magmatism at 750–755 Ma took place in continents that are commonly placed west of Laurentia in Rodinia (e.g., Li et al., 1995, 2004b; Torsvik et al., 2001; Yang et al., 2004). Including those in western and southern Laurentia, the spatial spread of the mamatism is too large to be explained by a single plume event. Li et al. (2003b) thus speculated that these mafic and felsic igneous suites could represent the manifestation of a Neoproterozoic mantle superplume (Fig. 13).

6. Conclusions

Dolerites from the 755 Ma Mundine Well dyke swarm crystallised from a common picritic parental magma that possessed geochemical and Nd–Hf isotopic characteristics closely resembling those of the plume-derived ocean island basalts. The MDS dolerites are similar in petrogenesis to similar-aged dolerite dykes from Seychelles and South China. They may thus have been generated by melting of a vast asthenospheric mantle plume (or mantle superplume) at ca. 750–755 Ma. This superplume event represents the later stage of the Rodinia superplume cycle that started continental rifting within Rodinia at ca. 820 Ma, and brought the breakup of the supercontinent by ca. 750 Ma (Li et al., 2003b).

Acknowledgements

We thank X.L. Tu, X.R. Liang, and Y.H. Yang for their help in trace element and Nd–Hf isotope analyses, and two anonymous reviewers for their comments which helped to improve the manuscript. X.H.L. thanks the NSC (Taiwan) for providing a 4-month visiting fellowship to the National Taiwan University. This work was supported by the NFSC (Grants 40273012 and 40421303). This is Tectonics Special Research Centre Publication No. 324, a contribution to IGCP 440.

References

Aleinikoff, J.N., Zartman, R.E., Walter, M., Rankin, D.W., Lyttle, P.T., Burton, W.C., 1995. U–Pb ages of metarhyolites of the Catoctin and Mount Rogers formations, central and southern Appalachians; evidence for two pulses of Iapetan rifting. Am. J. Sci. 295, 428–454.

Ashwal, L.D., Demaiffe, D., Torsvik, T.H., 2002. Petrogenesis of Neoproterozoic granitoids and related rocks from the Seychelles: the case for an Andean-type arc origin. J. Petrol. 43, 45–83.

Baker, J., Chazot, G., Menzies, M.A., Thirlwall, M.F., 1998. Metasomatism of the shallow mantle beneath Yemen by the Afar plume—implications for mantle plumes, flood volcanism and intraplate volcanism. Geology 26, 431–434.

Bhushan, S.K., 2000. Malani rhyolites—a review. Gondwana Res. 3, 65–77.

Bowden, P., Evans, D.A.D., Li, Z.X., Powell, C.M., 2001. Afro-Australian Precambrian anorogenic magmatism as indicators of supercontinental fragmentation. EUG 11, Strasbourg, France. J. Conf. Abstr. 6, 771.

Carlson, R.W., 1991. Physical and chemical evidence on the cause and source characteristics of flood basalt volcanism. Aust. J. Earth Sci. 38, 525–544.

Devlin, W.J., Brueckner, H.K., Bond, G.C., 1988. New isotopic data and a preliminary age for volcanics near the base of the Windermere Supergroup, northeastern Washington, USA. Can. J. Earth Sci. 25, 1906–1911.

Embleton, B.J.J., Schmidt, P.W., 1985. Age and significance of magnetisations in dolerite dykes from the Northampton Block, Western Australia. Aust. J. Earth Sci. 32, 279–286.

Ernst, R.E., Buchan, K.L., 1997. Giant radiating dyke swarms: their use in identifying pre-Mesozoic large igneous provinces and mantle plumes. In: Mahoney, J.J., Coffin, M.F. (Eds.), Large Igneous Provinces, Continental, Oceanic and Planetary Flood Volcanism. Geophysical Monograph 100. American Geophysical Union, Washington, DC, pp. 297–333.

Ernst, R.E., Buchan, K.L., 2001. Large mafic magmatic events through time and links to mantle-plume heads. In: Ernst, R.E., Buchan, K.L. (Eds.), Mantle Plumes: Their Identification Through Time. Geological Society of America, Special Paper 352, Boulder, pp. 483–575.

Evenchick, C.A., Parrish, R.R., Gabrielse, H., 1984. Precambrian gneiss and late proterozoic sedimentation in north-central British Columbia. Geology 12, 233–237.

Fetter, A.H., Goldberg, S.A., 1995. Age and geochemical characteristics of bimodal magmatism in the Neoproterozoic Grandfather Mountain Rift basin. J. Geol. 103, 313–326.

Frimmel, H.E., Kloetzli, U.S., Siegfried, P.R., 1996. New Pb–Pb single zircon age constraints on the timing of Neoproterozoic glaciation and continental break-up in Namibia. J. Geol. 104, 459–469.

Frimmel, H.E., Zartman, R.E., Späth, A., 2001. The Richtersveld igneous complex. South Africa: U–Pb zircon and geochemical evidence for the beginning of neoproterozoic continental breakup. J. Geol. 109, 493–508.

Gallagher, K., Hawkesworth, C., 1992. Dehydration melting and the generation of continental flood basalts. Nature 258, 57–59.

Gao, S., Liu, X.M., Yuan, H.L., Hattendorf, B., Günther, D., Chen, L., Hu, S.H., 2002. Determination of forty two major and trace elements in USGS and NIST SRM glasses by laser ablation-inductively coupled plasma-mass spectrometry. Geostandard Newslett. 26, 181–196.

Govindaraju, G., 1994. Compilation of working values and sample description for 383 geostandards. Geostandard Newslett. 18, 1–158.

Griffin, W.L., Pearson, N.J., Belousova, E., Jackson, S.E., van Achterbergh, E., O'Reilly, S.Y., Shee, S.R., 2000. The Hf isotope composition of cratonic mantle: LAM-MC-ICPMS analysis of zircon megacrysts in kimberlites. Geochim. Cosmochim. Acta 64, 133–147.

Hawkesworth, C.J., Mantovani, M.S.M., Taylor, P.N., Palacz, Z., 1986. Evidence from Paraná of South Brazil for a continental contribution to DUPAL basalts. Nature 322, 356–359.

Hawkesworth, C.J., Lightfoot, P.C., Fedorenko, V.A., Blake, S., Naldrett, A.J., Doherty, W., Gorbachev, N.S., 1995. Magma differentiation and mineralization in the Siberian continental flood basalts. Lithos 34, 61–88.

Hergt, J., Peate, D., Hawkesworth, C.J., 1991. The petrogenesis of Mesozoic Gondwana low-Ti flood basalts. Earth Planet. Sci. Lett. 105, 134–148.

Hickman, A.H., Lipple, S.L., 1978. Marble Bar, Western Australia. W. Aust. Geol. Surv., 1:250,000 Geol. Series Explan. Notes, p. 24.

Holm, O.H., Crawford, A.J., Berry, R.F., 2003. Geochemistry and tectonic settings of meta-igneous rocks in the Arthur Lineament and surrounding area, northwest Tasmania. Aust. J. Earth Sci. 50, 903–918.

Huang, S., Frey, F.A., 2003. Trace element abundances of Mauna Kea basalt from phase 2 of the Hawaii Scientific Drilling Project: petrogenetic implications of correlations with major element content and isotopic ratios. Geochem. Geophy. Geosy. 4 (Art. No. 8711).

Humayun, M., Qin, L.P., Norman, M.D., 2004. Geochemical evidence for excess iron in the Hawaiian mantle: implications for mantle dynamics. Science 306, 91–94.

Kelemen, P.B., Hanghoj, K., Greene, A.R., 2004. One view of the geochemistry of subduction-related magmatic arcs, with an emphasis on primitive andesite and lower crust. In: Rudnick, R.L. (Ed.), Treatise on Geochemistry, vol. 3. Elsevier Pergamon, Amsterdam, pp. 593–659.

Kieffer, B., Arndt, N., Lapierre, H., Bastien, F., Bosch, D., Pecher, A., Yirgu, G., Ayalew, D., Weis, D., Jerram, D.A., Keller, F., Meugniot, C., 2004. Flood and shield basalts from Ethiopia: Magmas from the African superswell. J. Petrol. 45, 793–834.

Lapen, T.J., Mahlen, N.J., Johnson, C.M., Beard, B.L., 2004. High precision Lu and Hf isotope analyses of both spiked and unspiked samples: a new approach. Geochem. Geophys. Geosyst. 5, doi:10.1029/2003GC000582, Q01010.

Lee, C.T., 2004. Are earth's core and mantle on speaking terms? Science 306, 64–65.

Lee, K.S., Chang, H.W., Park, K.H., 1998. Neoproterozoic bimodal volcanism in the central Ogcheon belt, Korea: age and tectonic implication. Precambrian Res. 89, 47–57.

Lee, S.R., Cho, M., Cheong, C.S., Kim, H., Wingate, M.T.D., 2003. Age, geochemistry, and tectonic significance of Neoproterozoic alkaline granitoids in the northwestern margin of the Gyeonggi massif, South Korea. Precambrian Res. 122, 297–310.

Li, X.H., 1997. Geochemistry of the Longsheng Ophiolite from the southern margin of Yangtze Craton, SE China. Geochem. J. 31, 323–337.

Li, X.H., Li, Z.X., Zhou, H., Liu, Y., Kinny, P.D., 2002. U–Pb zircon geochronology, geochemistry and Nd isotopic study of Neoproterozoic bimodal volcanic rocks in the Kangdian Rift of South China: implications for the initial rifting of Rodinia. Precambrian Res. 113, 135–154.

Li, X.H., Li, Z.X., Ge, W., Zhou, H., Li, W., Liu, Y., Wingate, M.T.D., 2003a. Neoproterozoic granitoids in South China: crustal melting above a mantle plume at ca. 825 Ma? Precambrian Res. 122, 45–83.

Li, X.H., Liu, D.Y., Sun, M., Li, W.X., Liang, X.R., Liu, Y., 2004a. Precise Sm–Nd and U–Pb isotopic dating of the super-giant Shizhuyuan polymetallic deposit and its host granite, Southeast China. Geol. Mag. 141, 225–231.

Li, X.H., Qi, C.S., Liu, Y., Liang, X.R., Tu, X.L., Xie, L.W., Yang, Y.H., 2005a. Petrogenesis of the Neoproterozoic bimodal volcanic rocks along the western margin of the Yangtze Block: new constraints from Hf isotopes and Fe/Mn ratios. Chin. Sci. Bull. 50, 2481–2486.

Li, X.H., Qi, C.S., Liu, Y., Liang, X.R., Tu, X.L., 2005b. Rapid separation of Hf from rock samples for isotope analysis by MC-ICPMS: a modified single-column extraction chromatography method. Geochimica 34, 109–114 (in Chinese with English abstract).

Li, Z.X., Zhang, L., Powell, C.M., 1995. South China in Rodinia: part of the missing link between Australia–East Antarctica and Laurentia? Geology 23, 407–410.

Li, Z.X., Li, X.H., Kinny, P.D., Wang, J., 1999. The breakup of Rodinia: did it start with a mantle plume benath South China? Earth Planet. Sci. Lett. 173, 171–181.

Li, Z.X., Li, X.H., Kinny, P.D., Zhou, H., 2001. Does it take a superplume to breakup a supercontinent? A case for Rodinia. In: Rodinia Symposium Perth, Geological Society of Australia, Perth, Australia, pp. 74–77 (Abstract 65).

Li, Z.X., Li, X.H., Kinny, P.D., Wang, J., Zhang, S., Zhou, H., 2003b. Geochronology of Neoproterozoic syn-rift magmatism in the Yangtze Craton, South China and correlations with other continents: evidence for a mantle superplume that broke up Rodinia. Precambrian Res. 122, 85–109.

Li, Z.X., Evans, D.A.D., Zhang, S., 2004b. A 90 degrees spin on Rodinia: possible causal links between the Neoproterozoic supercontinent, superplurne, true polar wander and low-latitude glaciation. Earth Planet. Sci. Lett. 220, 409–421.

Mahoney, J.J., 1988. Deccan Traps. In: Macdouogall, J.D. (Ed.), Continental Flood Basalts. Kluwer, Dordrecht, pp. 151–194.

McDonough, W.F., Sun, S.S., 1995. The composition of the earth. Chem. Geol. 120, 223–253.

McKenzie, D., O'Nions, R.K., 1991. Partial melt distributions from inversion of rare earth element concentrations. J. Petrol. 32, 1021–1091.

Nowell, G.M., Kempton, P.D., Noble, S.R., Fitton, J.G., Saunders, A.D., Mahoney, J.J., Taylor, R.N., 1998. High precision Hf isotope measurements of MORB and OIB by thermal ionisation mass spectrometry: insights into the depleted mantle. Chem. Geol. 149, 211–233.

Park, J.K., Buchan, K.L., Harlan, S.S., 1995. A proposed giant radiating dyke swarm fragmented by the separation of Laurentia and Australia based on paleomagnetism of ca. 780 Ma mafic intrusions in western North America. Earth Planet. Sci. Lett. 132, 129–139.

Parrish, R.R., Scammell, R.J., 1988. The age of the Mount Copeland syenite gneiss and its metamorphic zircons, Monashee Complex, southeastern Columbia, Radiogenic age and isotopic studies: report 2. Geol. Sur. Can. Paper 88-2, 21–28.

Pearce, J.A., Cann, J.R., 1973. Tectonic setting of basic volcanic rocks determined using trace element analyses. Earth Planet. Sci. Lett. 19, 290–300.

Plummer, P.S., 1995. Ages and geological significance of the igneous rocks from Seychelles. J. Afr. Earth Sci. 20, 91–101.

Powell, C.M., Preiss, W.V., Gatehouse, C.G., Krapez, B., Li, Z.X., 1994. South Australian record of a Rodinian epicontinental basin and its mid-Neoproterozoic breakup (approximately 700 Ma) to form the palaeo-Pacific Ocean. Tectonophysics 237, 113–140.

Preiss, W.V., 2000. The Adelaide Geosyncline of South Australia and its significance in Neoproterozoic continental reconstruction. Precambrian Res. 100, 21–63.

Rainbird, R.H., Jefferson, C.W., Young, G.M., 1996. The early Neoproterozoic sedimentary succession B of northwestern Laurentia: correlations and paleogeographic significance. GSA Bull. 108, 454–470.

Raczek, I., Jochum, K.P., Hofmann, A.W., 2003. Neodymium and strontium isotope data for USGS reference materials BCR-1, BCR-2, BHVO-1, BHVO-2, AGV-1, AGV-2F GSP-1. Geostandard Newslett. 27, 173–179.

Rhodes, J.M., Vollinger, M.J., 2004. Composition of basaltic lavas sampled by phase-2 of the Hawaii Scientific Drilling Project: geochemical stratigraphy and magma types. Geochem. Geophy. Geosy. 5 (Art. No. Q03G13).

Roeder, P.L., Emslie, R.F., 1970. Olivine–liquid equilibrium. Contrib. Mineral. Petrol. 29, 275–289.

Roots, C.F., Parrish, R.R., 1988. Age of the Mount Harper volcanic complex, southern Ogilvie Mountains, Yukon. Radiogenic age and isotope studies, report 2. Geol Sur. Can. Paper 88-2, pp. 29–35.

Russell, J.K., Nicholls, J., 1988. Analysis of petrologic hypotheses with Pearce element ratios. Contrib. Mineral. Petrol. 99, 25–35.

Sheppard, S., Occhipinti, S.A., Tyler, I.M., 2004. A 2005–1970 Ma Andean-type batholith in the southern Gascoyne Complex, Western Australia. Precambrian Res. 128, 257–277.

Stephens, W.E., Jemielita, R.A., Davis, D., 1997. Evidence for ca. 750 Ma intra-plate extensional tectonics from granite magmatism on the Seychelles: new geochronological data and implications for Rodinia reconstructions and fragmentation. EUG 9, Strasbourg, France. Terra Nova 9, 166.

Su, Q., 1994. Geochronological isotopic studies of late Proterozoic crossnore-type plutons in the Southern Appalachian Blue Ridge, North Carolina and Tennessee. Doctoral dissertation. University of North Carolina, Chapel Hill, NC, USA, p. 185.

Sun, S.S., McDonough, W.F., 1989. Chemical and isotopic systematics of oceanic basalt: implications for mantle composition and processes. In: Saunders, A.D., Norry, M.J. (Eds.), Magmatism in the Ocean Basins. Geological Society, Special Publication 42, pp. 528–548.

Tanaka, T., Togashi, S., Kamioka, H., Amakawa, H., Kagami, H., Hamamoto, T., Yuhara, M., Orihashi, Y., Yoneda, S., Shimizu, H., Kunimaru, T., Takahashi, K., Yanagi, T., Nakano, T., Fujimaki, H., Shinjo, R., Asahara, Y., Tanimizu, M., Dragusanu, C., 2000. JNdi-1: a neodymium isotopic reference in consistency with La Jolla neodymium. Chem. Geol. 168, 279–281.

Tatsumi, Y., Eggins, S.M., 1995. Subduction Zone Magmatism. Blackwell Science, Cambridge, p. 211.

Taylor, S.R., McLennan, S.M., 1985. The Continental Crust: Its Compositions and Evolution. Blackwell Scientific Publications, Oxford, p. 312.

Torsvik, T.H., Carter, L.M., Ashwal, L.D., Bhushan, S.K., Pandit, M.K., Jamtveit, B., 2001. Rodinia refined or obscured; palaeomagnetism of the Malani Igneous Suite (NW India). Precambrian Res. 108, 319–333.

Tucker, R.D., Ashwal, L.D., Torsvik, T.H., 2001. U–Pb geochronology of Seychelles granitoids: a Neoproterozoic continental arc fragment. Earth Planet. Sci. Lett. 187, 27–38.

Vervoort, J., Patchett, P.J., Blichert-Toft, J., Albarède, F., 1999. Relationships between Lu–Hf and Sm–Nd isotopic systems in the global sedimentary system. Earth Planet. Sci. Lett. 168, 79–99.

Wang, J., Li, Z.X., 2003. History of Neoproterozoic rift basins in South China: implications for Rodinia break-up. Precambrian Res. 122, 141–158.

Weis, D., Deutsch, 1984. Nd and Pb isotope evidence from the Seychelles granites and their xenoliths: mantle origin with slight upper-crust interaction for alkaline orogenic complexes. Isot. Geosci. 2, 13–35.

Wilson, M., 1989. Igneous Petrogenesis. Unwin Hyman Ltd., London, p. 466.

Wingate, M.T.D., Giddings, J.W., 2000. Age and palaeomagnetism of the Mundine Well dyke swarm, Western Australia: implications for an Australia–Laurentia connection at 755 Ma. Precambrian Res. 100, 335–357.

Xu, B., Jian, P., Zheng, H., Zou, H., Zhang, L., Liu, D., 2005. U–Pb zircon geochronology and geochemistry of Neoproterozoic volcanic rocks in the Tarim Block of northwest China: implications for the breakup of Rodinia supercontinent and Neoproterozoic glaciations. Precambrian Res. 136, 107–123.

Xu, X.S., O'Reilly, S.Y., Griffina, W.L., Zhou, X.M., 2003. Enrichment of upper mantle peridotite: petrological, trace element and isotopic evidence in xenoliths from SE China. Chem. Geol. 193, 168–188.

Yang, Z., Sun, Z., Yang, T., Pei, J., 2004. A long connection (750–380 Ma) between South China and Australia: paleomagnetic constraints. Earth Planet. Sci. Lett. 220, 423–434.

Zhao, J.X., McCulloch, M.T., Korsch, R.J., 1994. Characterisation of a plume-related ~800 Ma magmatic event and its implications for basin formation in central-southern Australia. Earth Planet. Sci. Lett. 121, 349–367.

Zhou, M.F., Yan, D.P., Kennedy, A.K., Li, Y.Q., Ding, J., 2002. SHRIMP U–Pb zircon geochronological and geochemical evidence for Neoproterozoic arc-magmatism along the western margin of the Yangtze Block, South China. Earth Planet. Sci. Lett. 196, 51–67.